Application of Numerical Methods to the Theory of the Periodic Deviations in the Schottky Effect*

GENEVA G. BELFORD,† ARON KUPPERMANN, AND T. E. PHIPPS
Noyes Chemical Laboratory, University of Illinois, Urbana, Illinois
(Received April 11, 1962)

Results are reported here for a new theoretical calculation of the periodic deviations from the Schottky line. Numerical methods exclusively were used to solve the Schrödinger equation for the emitted electron, to obtain transmission coefficients, and to calculate emitted current by averaging transmission coefficient over an appropriate electron energy distribution. The numerical calculations were carried out both for a simple-image-force potential barrier and for a similar potential differing only in having a small dip at the metal surface. Results for the simple-image-force potential were in complete agreement with previous analytic results, yielding Schottky deviations of approximately the right period and amplitude but shifted in phase by about a quarter-period from experimentally determined deviations. In disagreement with an earlier analytic-numerical study, results for the slightly altered potential were nearly identical to the simple-image-force results and showed the same phase shift.

1. INTRODUCTION

THE enhancement of thermionic emission from certain metals by the application of an external electric field is known as the Schottky effect.[1] This effect is easily explained as being due to a lowering (by the applied field) of the effective potential barrier close to the metal surface. The simple theory predicts a linear relationship between the logarithm of the emitted current and the square root of the field strength. However, very careful experimental work by Phipps and his co-workers[2,3] showed that the relationship is not quite linear—that, in fact, there exist periodic deviations from the so-called Schottky line. Since then there have been several theoretical attempts to explain this phenomenon, as well as additional experimental work.

The deviations were quickly recognized[4] to be a quantum mechanical effect due essentially to reflection of electrons having energies higher than the potential barrier maximum. The problem was to set up a reasonable model for the potential barrier at the metal surface, to solve the Schrödinger equation for this potential, and, finally, to obtain the emitted current from these wave-function solutions by averaging over an appropriate electronic energy distribution function. First of all, to make the problem tractable a one-dimensional model has always been assumed; that is, it is assumed that the metal surface is homogeneous and that the potential which the electron "sees" is simply a function of the distance from the surface. Secondly, the form of the potential barrier outside of the metal has been taken to be essentially that given by simple image force theory, based on a Coulombic attraction between the emitted electron and the positive "hole" it has left behind. Specifically, much theoretical work[5–8] was done on this problem using a potential of the form

$$\begin{aligned} V(x) &= -e^2/4x - eFx \quad \text{for} \quad x \geq x_1 \\ &= -W_a \quad\quad\quad\quad\ \text{for} \quad x \leq x_1; \end{aligned} \tag{1}$$

where $-e$ is the electronic charge, F is the electric field strength, x is the distance from the metal surface, $-W_a$ is equal to the sum of the Fermi energy and the work function, and x_1 satisfies the obvious continuity condition ($-W_a = e^2/4x_1 - eFx_1$). This potential, the so-called "simple-image-force potential," is pictured in Fig. 1. Approximate analytical solutions to the Schrödinger equation were obtained in various ways, and expressions for the Schottky deviations were derived. The results were encouraging in that theory and experiment agreed almost exactly on the period of the deviations and reasonably well on their amplitude. The theoretical deviations, however, differed in phase by about a quarter period from the experimental ones.

This phase difference indicated that perhaps a different model should be used for the potential at the metal surface. Herring[9] suggested that, based on theoretical work done by Bardeen,[10] a more realistic potential would feature a shallow potential well just at the metal surface and periodic behavior within the metal. This so-called Bardeen-Herring potential is also shown in Fig. 1. In looking at Fig. 1, one should keep in mind that the drawing is not to scale; in particular, the x scale is much expanded in the neighborhood of the origin to show the fine detail in the potentials in that area. In addition, Sachs and Dexter[11] have shown that the simple-image-force theory should have a quantum-mechanical correction term roughly proportional to x^{-2}. Drawing upon

* This work was supported in part by the U. S. Atomic Energy Commission and the University of Illinois Graduate Research Board.
† Postdoctoral Fellow, Division of General Medical Sciences, United States Public Health Service.
[1] W. Schottky, Physik. Z. **15**, 872 (1914).
[2] R. L. E. Seifert and T. E. Phipps, Phys. Rev. **56**, 652 (1939).
[3] D. Turnbull and T. E. Phipps, Phys. Rev. **56**, 663 (1939).
[4] H. M. Mott-Smith, Phys. Rev. **56**, 668 (1939).
[5] E. Guth and C. J. Mullin, Phys. Rev. **59**, 575 (1941).
[6] S. C. Miller and R. H. Good, Phys. Rev. **92**, 1367 (1953).
[7] D. W. Juenker, G. S. Colladay, and E. A. Coomes, Phys. Rev. **90**, 772 (1953).
[8] D. W. Juenker, Phys. Rev. **99**, 1155 (1955).
[9] C. Herring and M. H. Nichols, Revs. Modern Phys. **21**, 185 (1949).
[10] J. Bardeen, Phys. Rev. **49**, 653 (1936).
[11] R. G. Sachs and D. L. Dexter, J. Appl. Phys. **21**, 1304 (1950).

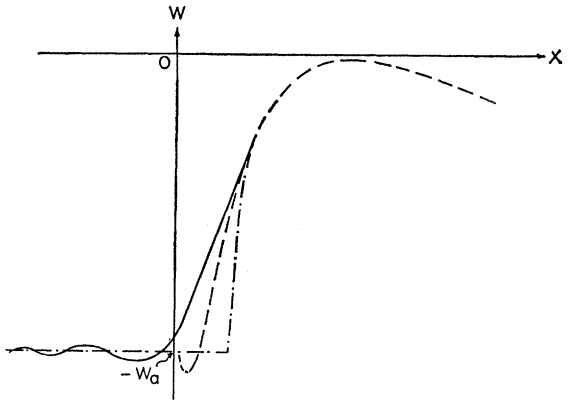

FIG. 1. Some proposed potential barrier models. Not drawn to scale. —·—· Simple image-force potential; —— the so-called Bardeen-Herring potential, adapted from Fig. 1 of Cutler and Gibbons (see reference 12); - - - - potential used by Cutler and Gibbons (see reference 12) and in the present work.

these ideas, Cutler and Gibbons[12] proposed a potential of the form (see Fig. 1)

$$\begin{aligned} V(x) &= -e^2/4x+\eta e^2/4x^2-eFx \quad \text{for} \quad x\geq x_c \\ &= -W_a \qquad\qquad\qquad\quad \text{for} \quad x\leq x_c, \end{aligned} \tag{2}$$

where x_c is the smallest real root of the equation

$$-e^2/4x+\eta e^2/4x^2-eFx=-W_a.$$

Using this potential and a combination of analytical and numerical techniques, they obtained excellent agreement with experiment for $\eta=0.0679$ Å, using a value $W_a=10$ eV, which is typical of several metals.

We decided to try to use completely numerical methods to compute the Schottky deviations; that is, we would begin by numerically integrating the Schrödinger equation and then we would use the wave functions obtained in this way to find the Schottky deviations. Numerical methods have the advantage of eliminating the need for analtyical oversimplifications. They should also be able to handle more complicated potentials which are analytically intractable. As a first step, however, we used virtually the same potential that Cutler and Gibbons used. Unfortunately our results are not in agreement with theirs. But we will leave discussion of results to a later section (Sec. 5) and now proceed to a description of our work. Section 2 contains the general theoretical background, while Secs. 3 and 4 consist of the details of our computations.

2. THEORY

Consider an electron moving in the one-dimensional potential given by Eq. (2). The Schrödinger equation describing the behavior of this electron is

$$-\frac{\hbar^2}{2m}\frac{d^2\Psi(x)}{dx}+[V(x)-W]\Psi(x)=0, \tag{3}$$

where W is the energy of the electron and Ψ is its wave function. When $V(x)$ is constant, this equation is exactly solvable. Therefore, for $x\leq x_c$ we can write the general solution

$$\Psi(x)=\frac{A}{[2m(W+W_a)]^{1/4}}\left[\exp\left(\frac{i}{\hbar}[2m(W+W_a)]^{1/2}x\right)+\mu\exp\left(-\frac{i}{\hbar}[2m(W+W_a)]^{1/2}x\right)\right], \tag{4}$$

where A and μ are complex numbers. Notice that the first term of Eq. (4) represents a wave moving from left to right; i.e., the original electron wave impinging on the barrier, while the second term represents a wave moving from right to left; i.e., the electron wave reflected from the barrier. In the region beyond the barrier we will have only a wave moving from left to right—a transmitted wave. Since at $x\gg x_s$ (where x_s is the location of the barrier maximum), $V(x)$ is a very slowly varying, almost linear function of x, in this region we may use the WKB approximation to write Ψ in the form

$$\Psi(x)=\frac{C}{\{2m[W-V(x)]\}^{1/4}}\times\exp\left(\frac{i}{\hbar}\int_{x_0}^{x}\{2m[W-V(x)]\}^{1/2}dx\right), \tag{5}$$

where C is, in general, a complex number and x_0 is chosen large compared to x_s. The transmission coefficient D and reflection coefficient R for electrons crossing the potential barrier from left to right are then given by

$$D(F,W)=|C|^2/|A|^2; \quad R(F,W)=|\mu|^2. \tag{6}$$

The numerical calculation of D and R proceeds in the following way. First, we select some value for the arbitrary constant C. We choose

$$C=\exp\left(-\frac{i}{\hbar}\int_{x_0}^{x_m}\{2m[W-V(x)]\}^{1/2}dx\right),$$

[where $x_m>x_0$ and x_0 is large enough for the approximation of Eq. (5) to be good], so that $|C|^2=1$ and $\Psi(x_m)$ is easily computed. Then, starting with this $\Psi(x_m)$, we integrate Eq. (3) inwards (in the direction of decreasing x) numerically. Notice that Ψ has a real and an imaginary part, but both satisfy Eq. (3) and are calculated completely independently. After the integration reaches the region where $V(x)=-W_a$, Ψ is compared with the form given by Eq. (4) and A and μ are extracted. This point will be discussed in greater detail in the next section.

The $D(F,W)$ obtained in this fashion represents the probability of transmission of an electron with energy W in field F. To find the total transmission probability, we must average $D(F,W)$ over the electron

[12] P. H. Cutler and J. J. Gibbons, Phys. Rev. **111**, 394 (1958).

energy distribution $N(W)$ to obtain

$$\langle D(F)\rangle=\left(\int_{-W_a}^{\infty} D(F,W)N(W)dW\right)\Big/\int_{0}^{\infty} N(W)dW. \tag{7}$$

The denominator here was selected on the basis of convenience from among the possible "normalizing" factors. Changing $\langle D(F)\rangle$ by a constant factor has no real effect on the final results, as we shall show later. We assume a Maxwellian energy distribution

$$N(W)=K\exp(-W/kT), \tag{8}$$

which is a very good approximation at the temperatures ($\sim$1500°K) at which experiments are usually performed. In this equation, K is a normalizing factor independent of W, T is temperature, and k is the usual Boltzmann constant.

Substituting (8) into (7), we obtain the following expression:

$$\langle D(F)\rangle=\int_{-W_a}^{\infty}\frac{D(F,W)\exp(-W/kT)dW}{kT}. \tag{9}$$

The actual theoretical thermionic emission current $i(F)$ is proportional to $\langle D(F)\rangle$, the constant of proportionality being independent of F.

The original Schottky theory assumes a transmission coefficient $D_s(F,W)$ which is zero for electrons with energies below the top of the barrier and unity for electrons with energies above the top of the barrier. The potential barrier is assumed to be that given by Eq. (1). Using $D_s(F,W)$ for D in Eq. (7), we obtain

$$\langle D_s(F)\rangle=\exp\{e^{3/2}F^{1/2}/kT\}. \tag{10}$$

The "Schottky" current $i_s(F)$ is proportional to $\langle D_s(F)\rangle$, the constant of proportionality being equal to the one relating $i(F)$ and $\langle D(F)\rangle$. Plotting $\log\langle D_s(F)\rangle$ vs $F^{1/2}$ does give us a straight line which is essentially the "Schottky line" mentioned in the introduction. Under the assumption that the experimental deviations from the Schottky line are caused by the difference between D and D_s, we obtain a theoretical deviation Δ as follows:

$$\Delta(F)=\log_{10}[i(F)/i_s(F)]=\log_{10}[\langle D(F)\rangle/\langle D_sF\rangle]$$
$$=\log_{10}\langle D(F)\rangle-\frac{e^{3/2}F^{1/2}}{kT\ln 10}. \tag{11}$$

It is the quantity $\Delta(F)$ that we wish to calculate numerically. This is then to be compared to the experimental quantity $\Delta_{exp}(F)$, defined by

$$\Delta_{exp}(F)=\log_{10}[i_{exp}(F)/i_{ref}(F)], \tag{12}$$

where $i_{exp}(F)$ is the measured emitted current in field F, and $i_{ref}(F)$ is an arbitrary reference line of slope $e^{3/2}/kT\ln 10$. The choice of intercept of this reference line has no effect on the important features of the deviation curve. It is this same arbitrariness that allows us a choice in selecting the normalizing factor of Eq. (7).

3. COMPUTATIONAL METHODS

A pair of computer programs were written for the Illiac (the University of Illinois' digital computer). The first of these outputs a table of $D(F,W)$ vs W when given the parameters defining the potential and the grid of W values required. The second program accepts a set of such tables for various F values, together with a value for the temperature, and outputs a table of the Schottky deviations vs F. The latter program simply integrates (using Simpson's rule) to obtain $\langle D(F)\rangle$ as given by Eq. (9), and then evaluates Eq. (11). The remainder of this section will therefore be devoted to a brief description of the program to calculate transmission coefficients.

Basic to the calculation of the transmission coefficient is the solution of the Schrödinger Eq. (3). (For computational convenience, Eq. (3) was first put into a form involving only dimensionless quantities.) It is important to use an integration method which is both accurate and very rapid. We selected a method due to Milne.[13] This is a fifth-order formula of the predictor-corrector type and is especially designed for second-order equations which have no first derivative term.

There were, however, certain programming difficulties which arose from this choice of method. Firstly, we needed to generate in some way the values of the solutions to the differential equation and their second derivatives at four points in order to start the calculation. Secondly, we wanted to change the mesh size Δx somewhere in the middle of the calculation. This is a simple procedure for, say, the Runge-Kutta method of solving differential equations, but is not readily done for predictor-corrector methods. The necessity for such a mesh change is fairly evident from the form of the potential (Fig. 1). At large distances from the metal surface the potential is a straight line of small slope, and fairly large values of Δx may be used. The size of Δx is limited, however, because Ψ is undulatory. Specifically, we see from Eq. (5) that at large x, when $V(x)$ is varying quite slowly, $\Psi(x)$ has a wavelength of about $h/\{2m[W-V(x)]\}^{1/2}$. Thus, for the typical case pictured in Fig. 2 ($W-V\approx 0.276$ eV) we see that the wavelength for $x\approx 200$ Å is approximately 23.3 Å. Close to the surface the potential varies rapidly, necessitating very small x increments. It is impractical to use a very small Δx throughout the calculation because of computer time limitations. Fortunately, a single program routine can be devised to take care of both setting up initial values and changing the mesh size. This consists of a routine which iterates initially given function values to obtain a set satisfying the differential equation at several points. The iterative formulas we used are given in Milne's book,[13] (p. 46). To start the calculation we

[13] W. E. Milne, *Numerical Solution of Differential Equations* (John Wiley & Sons, Inc., New York, 1953), p. 88.

"guess" initial function values, then iterate. (Of course, we are allowed to specify the value of the function and its derivative at one point.) To change the mesh size, we interpolate from function values obtained on the large mesh and then iterate, just as when starting the integration.

After accurate real and imaginary parts of Ψ have been obtained by integrating the differential equation (3), the next problem is to obtain the transmission and reflection coefficients from the values of $\Psi(x)$ for $x<x_1$. The form of the solution in this region is

$$\Psi(x)=\frac{A}{\varphi^{1/2}}\left[\exp\left(\frac{i\varphi x}{\hbar}\right)+\exp\left(-\frac{i\varphi x}{\hbar}\right)\right], \quad (13)$$

where $\varphi=[2m(W+W_a)]^{1/2}$. Let Ψ_z, A_z, and μ_z be the real parts of Ψ, A, and μ, respectively, and Ψ_y, A_y, and μ_y be the corresponding imaginary parts. Then evaluation of $\Psi(x)$ at the points $x=0$ and $x=-\pi\hbar/2\varphi$ yields the following set of simultaneous equations:

$$\begin{aligned}
\Psi_z(0)&=(A_z/\varphi^{1/2})(1+\mu_z)-(A_y/\varphi^{1/2})\mu_y;\\
\Psi_y(0)&=(A_y/\varphi^{1/2})(1+\mu_z)+(A_z/\varphi^{1/2})\mu_y;\\
\Psi_z(-\pi\hbar/2\varphi)&=(A_z/\varphi^{1/2})(1-\mu_z)-(A_z/\varphi^{1/2})\mu_y;\\
\Psi_y(-\pi\hbar/2\varphi)&=-(A_z/\varphi^{1/2})(1-\mu_z)-(A_y/\varphi^{1/2})\mu_y.
\end{aligned} \quad (14)$$

These equations are readily solved for the unknowns A_z, A_y, μ_z, and μ_y. From these quantities we calculate the transmission and reflection coefficients according to Eq. (6). In general, however, the points $x=0$ and $x=-\pi\hbar/2\varphi$ will not both lie on the grid on which we have solved the differential equation. It turned out to be quite satisfactory to choose the grid so that $x=0$ lies on it and then interpolate (using a fourth-order Stirling's formula) to obtain $\Psi(-\pi\hbar/2\varphi)$.

A check on the accuracy of the entire computation is provided by the relationship

$$D+R=1. \quad (15)$$

In a typical case, our calculation yielded $D+R=0.9999998$, which seemed sufficient accuracy for our purposes. As W increased, the deviation of $D+R$ from unity also increased, getting as large as 0.00002 for $W\approx 2$ eV; i.e., near the upper limit of W values for which the calculations were carried out (see Sec. 4.2). For these energy values, however, $N(W)$ is relatively small, so that the error in $D(W)N(W)$ (which is what we want to integrate) remains negligible.

4. COMPUTATIONS

4.1 Choice of Potential

Using a potential of the form given by Eq. (2), we are still free to vary the parameters W_a and η. W_a we chose to be 9.3 eV, corresponding to the value for tantalum, obtained from an experimental work function of 4.53 eV and a Fermi energy calculated[14] from an assumed free electron density of one electron per atom[5]. The form of the potential sets an upper limit on η of $e^2/16W_a$; for values of η larger than this the equation determining x_c has no real roots. Hence, in our case we are restricted to η 0.0965 Å. We used an η close to this limit, $\eta=0.090$ Å.

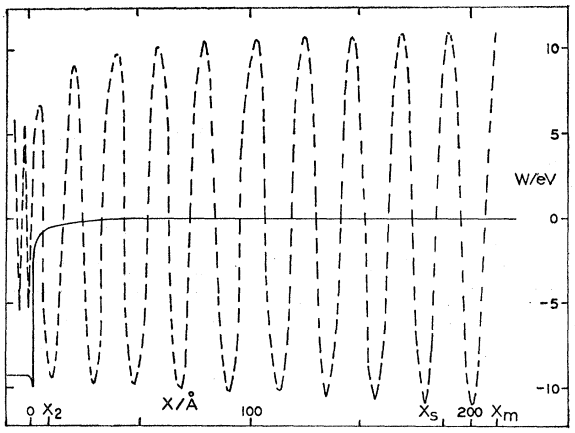

FIG. 2. Potential and a typical wave function for $F=9064$ V/cm, sketched to scale. Numerical results obtained with $\eta=0.090$ Å, $W_a=9.3$ eV. —— $V(x)$; ---- real part of wave function in arbitrary units, for an electron of energy 0.2716 eV.

Cutler and Gibbons,[12] whose results we wish to compare with ours, chose $W_a=10$ eV, a sort of average W_a for the three metals molybdenum, tungsten, and tantalum for which Schottky deviation data are available. They then selected η according to the rule $\eta=3e^2/64W_a$, which gives $\eta=0.0679$ Å. For $W_a=9.3$ eV, this rule yields $\eta=0.073$ Å, less than the value we used. Now, as η is increased, the dip in the potential curve becomes shallower and broader. Although the small difference between our potential and that of Cutler and Gibbons should not affect the results significantly, the broader potential that we use should be closer to the Bardeen-Herring[9,10] picture in which the potential oscillations inside the metal have a period of roughly interatomic size, implying a dip width of about 3 Å.

4.2 Program Parameters

To integrate Eq. (3) numerically, first we had to choose values for the following computational parameters: x_m, the large value of x at which the integration is started; $(\Delta x)_1$, the integration step for $x<x_2$; $(\Delta x)_2$, the integration step for $x>x_2$, and x_2, the step-change point. These parameters had to be selected by striking a balance between the requirements of accuracy and the restriction of computer time limitations. The values we decided upon are $x_m=212$ Å, $(\Delta x)_2=0.264$ Å, $(\Delta x)_1=0.033$ Å, and $x_2=8.46$ Å. In Fig. 2, we have indicated x_m and x_2 on plots of our potential for $F=9064$ V/cm and a typical resulting wave function.

[14] C. Kittel, *Introduction to Solid-State Physics* (John Wiley & Sons, Inc., New York, 1953), p. 229.

It is clear that although we have not really chosen $x_m \gg x_s$, as we required in the discussion of Sec. 2., the WKB approximation should still be good near this x_m throughout most of our energy range. Specifically, the criterion for the applicability of the WKB approximation is[15]

$$B \equiv \hbar m(\partial V/\partial x)/[2m(W-V)]^{3/2} \ll 1. \quad (16)$$

A rough calculation shows that $B<10^{-3}$ for $F \approx 10^4$ V/cm and $W-V>0.0015$ eV. The difficulty that arises as $W-V$ decreases through zero and becomes negative is taken care of in our program by an automatic temporary increase in x_m. Tests on selected cases indicated that increasing x_m or x_2, or decreasing $(\Delta x)_1$ or $(\Delta x)_2$, does not significantly affect the results.

In the numerical integration of Eq. (9) it is evident that the practical limits on the integration are not from $-W_a$ to ∞, but from a point where $D(F,W)$ is negligibly small to where $\exp(-W/kT)$ is negligibly small. We therefore fixed the upper limit at $W_{\max}=1.922$ eV. This corresponds to $\exp(-W/kT)=3\times10^{-7}$ for $T=1500°$K. Since the lower limit for W must lie under the barrier top, at some small *negative* value of W, at $W_{\max}$ the electron density has fallen off to about 10^{-7} of its maximum value. The lower integration limit $W_{\min}$ was adjusted so that $D(F,W_{\min})<10^{-9}$. The region of integration was initially cut up into about 40 segments for the application of Simpson's rule. However, D changes abruptly in the immediate vicinity of the barrier maximum, (see Sec. 5), and a much finer grid is required there. Thus, a typical table of $D(F,W)$ consisted of about 39 points for $W=W_{\max}-n\Delta W$ ($n=0$, 1, $2\cdots38$; $\Delta W \approx 0.053$ eV), plus some 50 to 100 points for $W=W_c-2^{-5}m\Delta W$ ($W_c=W_{\max}-38\Delta W$; $m=0,1\cdots$).

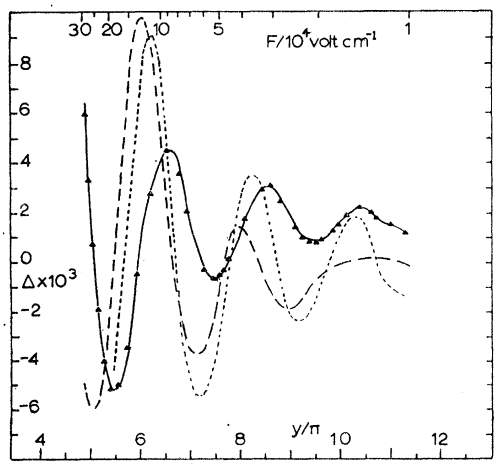

FIG. 3. Periodic deviations from the Schottky line. - - - - Experimental curve for tantalum, adapted from Seifert and Phipps (see reference 2), Fig. 5. · · · Theoretical curve, Cutler and Gibbons (see reference 12). ▲ Numerically calculated points, this work, $\eta=0.090$ Å. (For purposes of comparison, a curve has been sketched connecting these points.)

[15] D. Bohm, *Quantum Theory* (Prentice-Hall, Inc., New York, 1951), p. 267.

Again, we adjusted the parameter values until further refinements caused insignificant changes in the results. For example, for low F values, where D varies especially rapidly with W, we found we had to choose $W=W_c-2^{-6}m\Delta W$, when $W \leq W_c$.

Tables of $D(F,W)$ were obtained for 35 values of F over the range 9064 V/cm$\leq F \leq 2.63\times10^5$ V/cm. Since such a table took 1 to 2 h to compute (about 2 min per point), it is evident that anything in the way of a general refinement of mesh parameters or a complication in the potential would quickly make the computational time prohibitive on Illiac (which has a multiplication time of about 700 μsec). It is for this reason also that we were unable to do much in the way of varying, for example, the parameters in the potential.

5. RESULTS

5.1 Periodic Deviations

In Fig. 3 we have plotted the main result of our work, a curve of the Schottky deviations Δ, computed as described in the preceding sections, as a function of field. Since theoretical workers[6,7,8,12] discovered Δ to be proportional to a periodic (cosine) function of the variable $y=4e^{5/4}m^{1/2}/3\hbar F^{1/4}=357.1\ (V/\text{cm})^{1/4}/F^{1/4}$, we have used y as the abscissa in Fig. 3. For comparison purposes, Fig. 3 also contains an experimental curve and the results of Cutler and Gibbons.[12]

In comparing these curves, recall that the location of the line $\Delta=0$ is arbitrary for all three curves, so that it is only their absolute amplitudes and phases that should be compared. Notice that our curve differs considerably from both the experimental curve and that of Cutler and Gibbons. This last is particularly surprising in view of the fact that we have used a model virtually identical to that used by them. (cf. Secs. 1 and 4). Our results, however, agree very well with the old results given by simple-image-force theory. (The agreement is so close that we have not bothered to include an image-force-theory curve in Fig. 3.)

The explanation of these facts that comes to mind most readily is that the dip in the potential introduced by Cutler and Gibbons is not really large enough to affect the Schottky deviations and that Cutler and Gibbons' good results somehow arise spuriously from their analytical approximations. An alternate possibility was that our numerical integration was ignoring the dip, but we ruled this out to our satisfaction by drastically cutting down the integration mesh-step Δx in the vicinity of the dip and noting only an insignificant change in the resulting Δ. To test this point further, we obtained some points for the same potential form but with $\eta=0$. Setting $\eta=0$ should just eliminate the dip and yield the simple image force theory results. A considerable difference was obtained between the Δ values computed for $\eta=0$ and those for $\eta=0.09$ Å. *However*, the entire difference consisted of a very small decrease in the amplitude of the deviations, coupled with what we can consider as a shift

of 0.0005 (quite sizable) in the $\Delta=0$ base line. This is excellent corroborating evidence that our computational method is not just ignoring the potential dip. The calculations show, in fact, that the dip simply causes a uniform increase in the amount of emitted current (i.e., a shift of base line) but has virtually no effect on the phase or amplitude of the periodic deviations. For further discussion on this point, see Sec. 5.3.

5.2 Temperatue Dependence of Periodic Deviations

It is of some interest to investigate the temperature dependence of the periodic deviations. Theoretical workers[6,8,12] have been in agreement that the amplitude of the periodic deviations should vary linearly with T^{-1}, while the phase should have no T dependence. Experimentally, the deviation amplitude is determined with

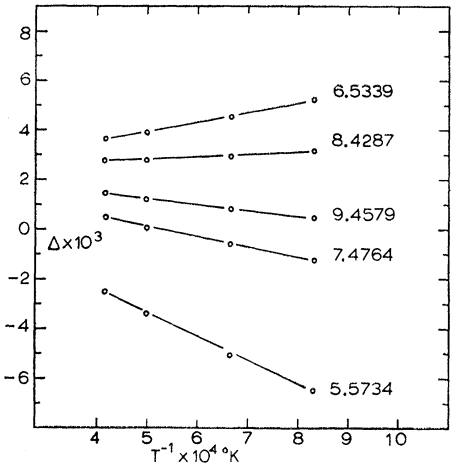

FIG. 4. Plot of Δ vs T^{-1} for several values of the field. The number identifying each curve is the corresponding y/π. The straight lines are drawn to indicate the approximate linearity of the points.

a relatively large uncertainty of about 20%[16]; within this uncertainty, the dependence of amplitude on temperature agrees with theory, while it has been a moot point whether or not some variation of phase with temperature can be seen.

Our numerical work is in complete agreement with previous theoretical studies. In Fig. 4, Δ vs T^{-1} for several values of F was plotted. The general linear dependence is evident, although there is a slight deviation from linearity. The deviation is probably within the range of the computational accuracy. Notice that, in agreement with the fact that it is the *amplitude* of the Schottky deviations which increases with increasing T^{-1}, Δ increases (with T^{-1}) in the neighborhood of maxima and decreases in the neighborhood of minima.

The very nature of numerical work, in which only discrete points are obtained, makes it difficult to study small phase shifts. This same difficulty, of course, arises in experimental work. The best we can do is to examine the temperature variation of several very closely spaced points in the vicinity of a maximum or a minimum. The result of our doing this is shown in Fig. 5. Clearly any phase shift with temperature must be either *very* small or nonexistent.

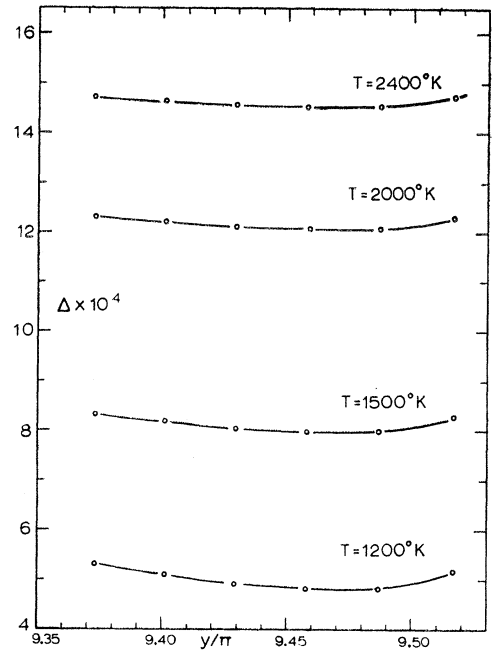

FIG. 5. Close examination of one minimum in the Δ vs y curve for several T values, in order to detect a phase shift, if any exists, with changing T.

5.3 Transmission Coefficients

As a by-product of calculating the Schottky deviations, we obtained extensive tables of the transmission coefficient $D(W)$ for a series of values of the field F; i.e., for a series of potential barriers very similar to each other in form. Some unexpected features appeared in these results which we feel merit interest in their own right and which also may shed some light on the Schottky deviations.

Firstly, the general behavior of $D(W)$ as a function of W is about what one would expect. As the electron energy approaches W_b (the energy corresponding to the top of the potential barrier) from below, $D(W)$ rises very sharply from zero to about 0.96, which is reached for W slightly greater than W_b. From this point the rise in $D(W)$ proceeds at a much slower rate, appearing nearly linear over small ranges of W (but of course $D(W)$ eventually approaches 1.00 asymptotically). Previous workers have obtained much the same sort of thing. (See, for example, Fig. 2 in the paper[5] by Guth and Mullin.)

The really interesting feature is the detailed behavior

[16] G. A. Haas and E. A. Coomes, Phys. Rev. **93**, 1421 (1954).

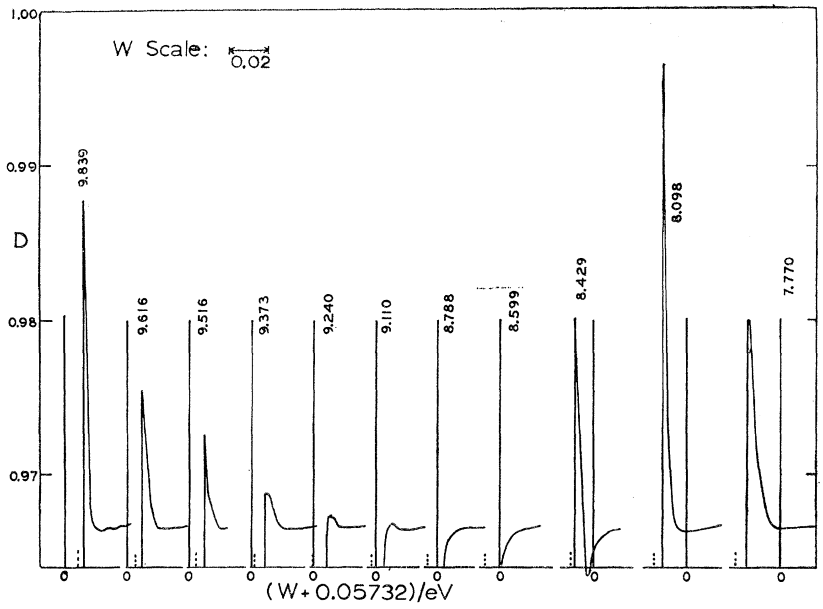

FIG. 6. $D(W)$ for several values of field, all plotted with respect to the same arbitrary zero of energy. The number above each graph gives the value of y/π. ⋮ denotes the position of the corresponding barrier height W_b.

of $D(W)$ for W just slightly larger than W_b. In this region $D(W)$ appears to oscillate. This fact is not in itself strange, since such oscillations are a common feature of the most simple potential barrier problems. What is noteworthy is that for some values of F these oscillations are very large, while for other values of F the oscillations practically vanish. Furthermore, the waxing and waning of these oscillations can be roughly correlated with the periodicity of the Schottky deviations. To illustrate this, in Fig. 6 we have plotted $D(W)$ vs W, in the vicinity of W_b, for several values of y/π varying over approximately one Schottky deviation period. Notice that we start with a rather high, sharp peak, which gradually decreases in height and broadens as y decreases until no peak is visible at all. Then a new peak rises very rapidly, beginning as a small shoulder on the side of the broadened-out old peak. (This last feature is shown more clearly in Fig. 7.) The new peak begins to decline and broaden, and the cycle is complete. This same pattern is repeated over the other Schottky deviation periods. Of course, the rise and fall of the peaks is superimposed on a gradual shift toward lower energies, corresponding to the lowering of the barrier height with increasing field (decreasing y). Outside the region of the peak the rise of D to unity was identical throughout the range of fields considered.

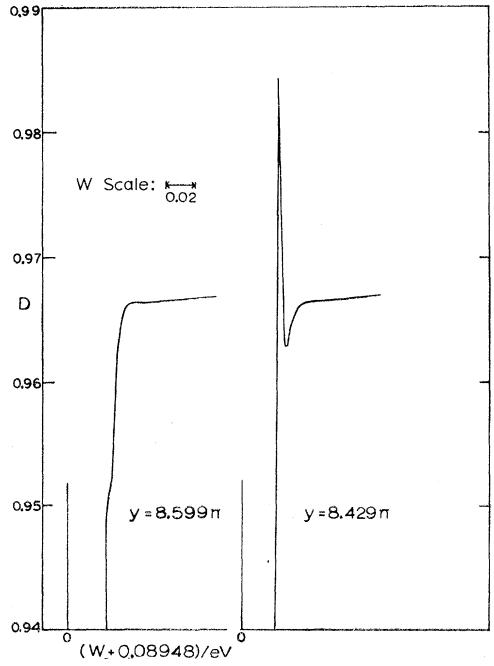

FIG. 7. $D(W)$ for two values of field, showing in detail the rapid rise of a sharp peak from a shoulder.

It seems reasonable to conclude, therefore, that the oscillating peak in the $D(W)$ curve is the direct cause of the Schottky deviations. Other workers have attributed the deviations to interference between electron waves reflected from various parts of the potential barrier.[4–9,12] Our results are entirely consistent with this, since the periodic variation in the transmission peak has the earmarks of an interference effect. In fact, a careful investigation of the correlation between the oscillations of the transmission peak and the changing potential may yield clues as to exactly what regions of the potential are responsible for the interfering reflections and, furthermore, what alteration of the form of the potential might bring about the desired phase shift. We have not as yet come to any conclusions along these lines.

All of the results presented in Figs. 2–7 have been obtained with the potential given by Eq. 2 with $\eta=0.090$ Å. Now, in Fig. 8, we contrast a plot of $D(W)$ for

$\eta=0.090$ Å with one for $\eta=0$ (simple image force). As we mentioned in Sec. 5.1, the effect of setting $\eta=0$ is simply to shift the whole curve by a nearly constant amount. Although we have here plotted D for only one value of field, the same result held for other field values checked. Since the rise and fall of the transmission peak, which correlates with the periodic Schottky deviations, does not appear to be significantly affected by the change from $\eta=0.090$ Å to $\eta=0$, we would not expect the $\eta=0.090$ Å potential to yield Schottky deviations shifted in phase from those given by simple image force theory.

We have been discussing a single "transmission peak," but it is interesting to note in Fig. 8 that in addition to one tall peak there are several smaller oscillations appearing at slightly larger energies. These extra oscillations appear only at the smallest field (largest y) values, damping out to the point of being barely visible (cf. Fig. 6) when $y/\pi=9.839$ (i.e., $F=1.782\times10^4$ V/cm).

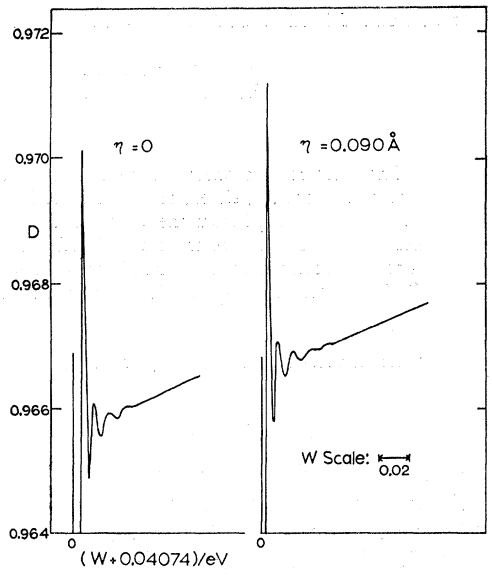

FIG. 8. $D(W)$ for $y=11.317\ \pi$, for two different values of the potential parameter η.

6. CONCLUSIONS

The principal conclusion of our work is that the periodic deviations in the Schottky effect are far from being thoroughly understood. Our results, in contradiction to those of Cutler and Gibbons, demonstrate that the potential of Eq. (2) is no more adequate than the simple image-force potential to explain the phase of the Schottky deviations. Undoubtedly, a more complicated potential form is needed; at least, there appears to be no simple variant of Eq. (2) which changes the potential in any important respect. Since a potential of the complexity of Eq. (2) already pushes both analytic methods and high-speed computer methods near their practical capability limits, further work involving more complex potentials will probably require the use of the higher speed computers now coming into common use.

ACKNOWLEDGMENTS

The authors wish to thank Dr. J. Blankfield for a preliminary investigation of some of the computer programming difficulties, and Mr. J. Lockhart for calculating the W_b values shown in Fig. 6.